Distinct and Asymmetric Neuronal Responses to Pitch- and Roll-Axis Vestibular Stimulation in larval zebrafish

Geoffrey Migault*[1], Natalia Beiza-Canelo*[1], Sharbatanu Chatterjee*[1], Georges Debrégeas[1], and Volker Bormuth[1,✉]

[1]Sorbonne Université, CNRS, Institut de Biologie Paris-Seine (IBPS), Laboratoire Jean Perrin (LJP), Paris, France
*equal contribution

The vestibular apparatus plays a pivotal role in maintaining postural equilibrium and processing movement signals, underscoring its importance in the study of certain neurological disorders. Here, we present a rotating light-sheet microscope, enabling brain-wide functional recordings during dynamic vestibular stimulation along both the roll and pitch axes in head-restrained zebrafish larvae. The system incorporates a double galvanometer mirror configuration, is amenable to 3D printing, and enhances scanning efficiency. Employing this apparatus, we have successfully conducted the first comprehensive mapping of zebrafish brain responses to dynamic pitch-tilt vestibular stimulation. Through Fourier and regression analyses, we report an asymmetry in neuronal recruitment during nose-up versus nose-down pitch tilts within critical regions including the cerebellum, oculomotor nucleus, caudal hindbrain, and vestibular nucleus, highlighting physiological adaptations to downward motion. We identified specific brain regions, notably the cerebellum and medial-rostral rhombencephalon, that exclusively respond to roll- but not pitch-tilt vestibular stimuli. Furthermore, we have identified a transgenic line that closely correlates with our functional mappings and demonstrates a significant response to vestibular stimulation. The elucidation of brain-wide neuronal circuits involved in vestibular processing establishes a foundational framework for subsequent detailed investigations into the molecular and genetic mechanisms underlying postural control and motion perception.

Light-sheet functional imaging | Vestibular processing Vestibular processing | Light-sheet functional imaging | Rotating light-sheet microscopy | Larval zebrafish

Correspondence: ***volker.bormuth@sorbonne-universite.fr***

Introduction

The vestibular apparatus is a critical sensory system in animals, essential for maintaining postural control, perceiving spatial orientation, and responding to movement cues. It plays a fundamental role in coordinating motor behaviors, crucial for balance and spatial awareness. Dysfunction in this system is associated with various neurological disorders such as Alzheimer's disease, Parkinson's disease, progressive supranuclear palsy, and autism spectrum disorder (1–4), underscoring the importance of understanding its mechanisms at the brain-wide circuit level. Recent advances in imaging techniques have provided opportunities to explore brain-wide neural activity related to vestibular processing. For instance, a miniaturized rotating light-sheet microscopy approach (5) allows comprehensive brain-wide neuronal recordings during controlled vestibular stimulation in larval zebrafish. Other methods include tilting fish under a static microscope (6), rotating them with the microscope objective (7, 8), and creating fictive vestibular stimuli by exerting forces on the otoliths with optical tweezers (9) or utilizing magnets following ferrofluid injection into the otic vesicle (10). Comprehensive brain wide neural responses have only been characterized for the roll-tilt axis. In contrast, investigations of pitch-tilt responses have been confined to distinct sparse neural subpopulations (6, 11), leaving the broader, pan-neuronal correlates associated with pitch-tilt stimulation unexplored.

This study introduces significant enhancements to the miniaturized rotating light-sheet microscope approach, enabling precise rotations along axes between roll and pitch tilt directions with simultaneous whole-brain imaging. Our novel design, which is 3D printable and easy to assemble and reproduce, features a double galvanometer mirror configuration, enhances scanning capabilities. This advancement allows us to examine larval zebrafish responses to vestibular stimulation on the pitch-tilt axis and compare them to the roll-tilt response, an aspect of vestibular processing previously unexplored with whole-brain imaging.

Maintaining postural control along the pitch-tilt axis is critical for survival, often closely tied to the initiation of movement. For instance, organisms need to lean forward to start moving, causing disbalance, which needs to be compensated. This balancing act, especially against acceleration and deceleration forces, is crucial. Larval zebrafish present a unique case in this context. As demonstrated by Ehrlich et al. (12) they experience inherent postural instability along the pitch axis, attributed to the misalignment between their center of buoyancy and center of gravity. This misalignment leads to a consistent nose-down postural destabilization. To counteract this, larval zebrafish perform active righting movements, accompanied by changes to pitch angle to maintain their posture. Notably, the initiation of their characteristic swim behavior patterns is directly influenced by their vestibular system's detection of this destabilization. This highlights the evolutionary necessity for developing efficient neuronal pathways that compensate for pitch-axis postural control and its related movement complexities.

Our primary objective was to determine if distinct neuronal responses and potential asymmetries exist in processing nose-up and nose-down tilt directions, given the behavioural

ubiquity of the nose-up tilt direction movements used in righting movements. We also recorded responses to roll-tilt stimuli in the same animals to compare the spatial organization of neuronal populations between pitch-tilt and roll-tilt axes. This offers insights into how different vestibular stimulations differentially activate brain regions.

Results

Enhanced Light-Sheet Microscopy for Diverse Vestibular Stimulation. The light-sheet unit is an advanced version of the setup detailed by Migault et al. (5). Modifications include a 3D printable bracket and a dual galvanometer mirror setup. The system utilizes a 488 nm laser beam delivered via an optical fiber. This beam, first collimated by a 5x objective (numerical aperture 0.16), is directed to the first galvanometer mirror, enabling z-directional light sheet translation. The beam then reaches the second galvanometer mirror, oscillating at 400 Hz, creating a light sheet parallel to the imaging plane.

The core of this unit is a specially designed bracket, central to securing the objectives and mirrors in place. This arrangement is illustrated in Figure 1, and the 3D design file is open source and can be accessed at https://a360.co/2U1KBoH. For ease of adjustment, the objectives are clamped rather than screwed, which ensures precise positioning of the optical fiber output and the laser beam for optimal collimation. Additionally, the illumination objective's translation feature simplifies the alignment of the laser beam's waist with the observation objective's field of view center.

To broaden the scope of vestibular stimulation directions, we mounted both the light-sheet unit and the sample holder on a compact, rotatable platform. This platform's rotation axis, depicted as a green dotted line in Figure 1C), is aligned with the detection objective's optical axis. By rotating and then securing this element with a fixation screw, we defined the axis around which the fish tilts when the entire microscope rotates. Consequently, we could switch the vestibular stimulation direction from a roll-tilt (Figure 1C) to a pitch-tilt (Figure 1D) configuration. Crucially, during these manipulations, the fish consistently stays within the microscope's field of view. Also, as the light-sheet unit shares the rotating platform with the sample chamber, it always maintains a lateral orientation relative to the fish. This setup enables us to consistently obtain sharply focused images of the same neurons by merely adjusting the vestibular stimulation axis while keeping the illumination uniform. Such a configuration is instrumental in allowing us to make direct comparisons between the neuronal responses to roll and pitch-tilt stimulations.

To achieve mechanical stability in the 3D printed unit, we reinforced it with a thin aluminum plate on one side. This modification ensures an ultra-stable setup, limiting movement in the x and y directions to less than 2 μm and in the z-direction to less than 500 nm, as depicted in Figure S1C.

Comparing brain-wide neuronal correlates of pitch- and roll-tilt stimuli. .

Neural Responses Induced by Sinusoidal Pitch-Tilt Stimuli. Utilizing our improved system, we investigated the brain's neuronal response to pitch-tilt vestibular stimulation. Animals were subjected to a sinusoidal rotation around their horizontal dorsal up orientation, at a frequency of 0.2 Hz and an amplitude of ±20°, for 10 minutes (120 periods). A substantial number of neurons responded to this stimulation, as showcased in Video .

We successfully mapped brain-wide neuronal responses by employing Fourier analysis to pinpoint neurons showing significant activity at the stimulus frequency. The phase of these responses was analyzed relative to the stimulus waveform's phase, revealing the intricate dynamics of neuronal activity. Importantly, we corrected for delays caused by the calcium sensor to determine the actual neural response phase (see STAR Methods for methodology details). Our analysis across the brain revealed a spectrum of phase shifts, peaking around $\pi/3$ and $4\pi/3$, as shown in Figure 2A. To visualize the spatial distribution of neurons based on their response phases we color-coded them to create phase maps depicted in Figures 2C-F and 3D animated in Video . Here, color coding represents phase shift values, and pixel intensity indicates response amplitude.

The response maps exhibited a mirror-symmetrical layout around the sagittal midplane. For enhanced clarity, we displayed the phase map of a typical fish in four separate phase windows using z-projections (Figure 2B), with Figure 2A illustrating how phases were allocated for each window spanning a phase and its direct 180° opposite. Remarkably, within each window, the neuronal populations displaying responses 180° out of phase with each other show distinct and separated spatially organized patterns. We centered the first phase window around $\pi/3$ and $4\pi/3$, where we observed the largest response amplitudes. Figure 2C shows the mean neural activities of these so-defined neuronal clusters illustrating how they are tuned to different parts of the stimulus cycle. Neurons in the phase window (i), which encompassed most of the neurons, exhibited a mixed tonic-phasic response, indicating sensitivity to both the position and the angular velocity of the stimulus, as demonstrated by the average neuronal responses shown in Figure 2B. These average responses were tuned to nose-up tilt (red) and nose-down tilt (cyan). To facilitate a deeper comprehension of the three-dimensional organization, we show single-layer views of the full phase maps for four selected layers in Figure 2C. Strikingly, the response patterns we found are stereotypical among different animals, as shown by the computed averaged phase maps from recordings in 8 fish (Figure 2F).

Localized neuronal activity was observed in the tegmentum, encompassing the nucleus of the medial longitudinal fascicle (nMLF), oculomotor and trochlear nuclei, as well as in the cerebellum and the rhombencephalon, particularly in the octavo-lateral nucleus regions adjacent to the otic vesicles. This region includes the tangential and medial vestibular nuclei and vestibulo-spinal backfill neurons. Furthermore, the inferior olive and parts of rhombomere 7 were responsive.

In the tegmentum, we found that the trochlear nucleus (nIV)

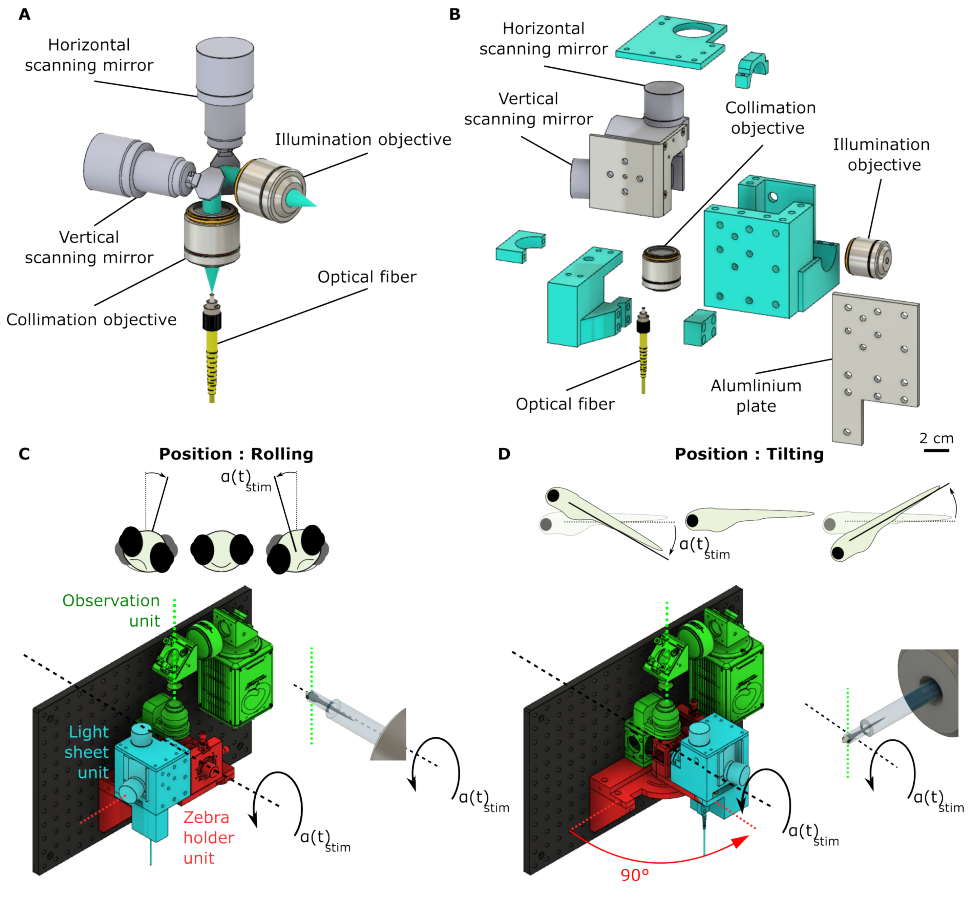

Fig. 1. The Experimental Setup. (A) Schematic representation of the optical elements that define the laser path in the light-sheet unit, with the laser path highlighted in blue. (B) Exploded view of the light-sheet unit, displaying the 3D printed components in cyan. The metal plate (gray) is securely attached to the 3D-printed bracket to enhance the mechanical stability of the unit during microscope rotations. (C) Full view of the light-sheet microscope setup: The light-sheet unit is depicted in blue, the specimen holder in red, and the detection unit in green. These components are mounted on a breadboard that is fixed to a high-speed precision rotation stage. To allow arbitrary changes between the roll-tilt and pitch-tilt configurations for vestibular stimulation, the light-sheet unit and the sample holder were placed on a small rotatable platform. The position of this element was adjusted to define the axis around which the fish was tilted when the entire microscope was rotated. The configuration displayed here demonstrates a vestibular roll-tilt stimulus. (D) The configuration displayed here demonstrates a vestibular pitch-tilt stimulus. See also Figure S1

notably responded solely to nose-upward movements. The oculomotor nucleus (nIII) displayed a differentiated response pattern: its lateral part was activated by nose-up movements, while the medial part reacted to nose-down movements. This asymmetry in oculomotor neuron activation in nIII and nIV aligns with findings from recent backtracing studies mapping these neurons to their specific oculomotor muscle targets (14). The functional responses' spatial organization reflects the projection patterns of these ocular motor neurons, which are pivotal for controlling eye rotations during pitch-tilt movements of the body, either nose-up or nose-down (see Figure 2D and Figure S3). Specifically, during nose-up rotations, the nIV nucleus, targeting exclusively the superior oblique eye muscles, in conjunction with the lateral part of nIII, which innervates the inferior rectus eye muscles, coordinates upward eye rotations. In contrast, nose-down pitch-tilt movements activate nIII's medial part, associated with the superior rectus and inferior oblique eye muscles, facilitating downward eye movements.

Finally, in the caudal hindbrain, a medial-dorsal cluster of neurons responded to nose-up movements, flanked by two laterally located strips of neurons tuned to nose-down movements (Figure 2F).

Neural Responses to Sinusoidal Roll-Tilt Stimuli in the Same Fish. Beyond documenting the tilt response, we also captured the roll response in all fish in response to a sinusoidal rotation along the roll-tilt axis with an amplitude of ±10° around their preferred dorsal-up posture. Phase maps corresponding to these roll responses are depicted in Figure 2G-H and video 3.

The pitch-tilt and the roll-til stimulus recruited globally the same brain regions, including the optic tectum, habenula, cerebellum, tegmentum, oculomotor nucleus III, trochlear nucleus, medial longitudinal fasciculus nucleus, tangential nucleus, inferior olive, and rhombomeres Rh1 to Rh7.

We observed significant differences between the roll- and pitch-tilt responses (Fig. 2.E and Fig. 2.G).

While both responses are mirror-symmetric to the sagittal midplane, the roll-tilt response shows a distinctive 180-degree phase shift in neuronal responses between the two brain hemispheres.

We observed populations of neurons in the cerebellum that responded only to the roll-til stimulus (Figure 2G dashed oval compared to F) and in general fewer cerebellar neurons were recruited during the pitch-tilt stimulus.

Additionally, the medial-rostral part of the rhombencephalon exhibited exclusive responsiveness to the roll-tilt stimulus.

Vestibular spinal neurons were strongly activated on each brain side during roll- and pitch-tilt stimulation (see arrowheads 2. F-H). However, during pitch-stimulation, these neurons demonstrated tuning to nose-down rotations without a response to nose-up movement, while during roll tilt, they displayed tuning to ipsilateral ear-down rolls respectively.

Furthermore, we observed during both stimulation directions recruitment of a population of neurons in the tegmentum ros-

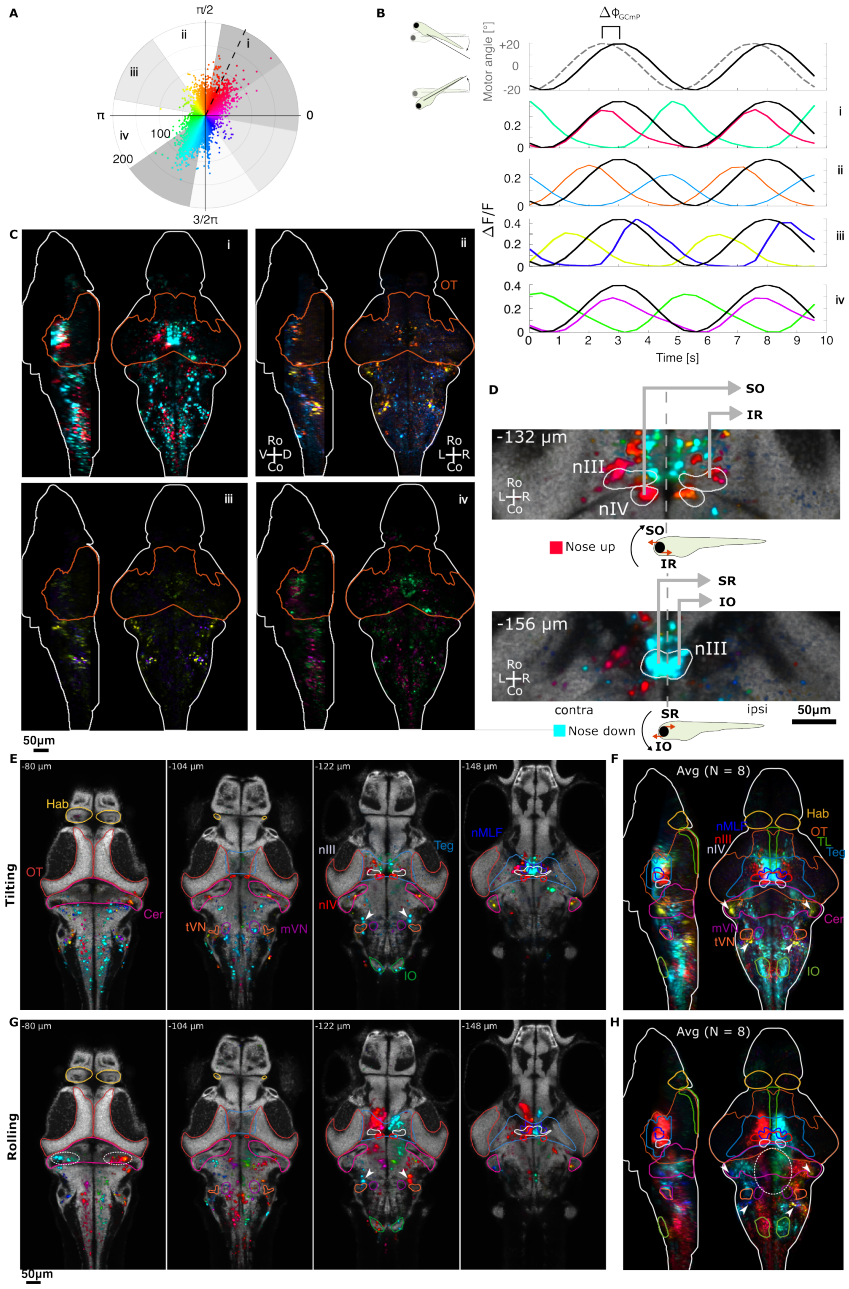

Fig. 2. Neuronal Response Maps to Sinusoidal Pitch- and Roll-Tilt Stimulation. (A) Polar plot displaying neuron fluorescence response amplitude, measured in signal-to-noise ratio units at the stimulation frequency, plotted against the response phase delay relative to the stimulus. Phase delays were adjusted for the 1.15 radians phase delay introduced by the GCaMP6f sensor (STAR Methods). The dotted line marks the zero phase shift position before correction. Phase delays are color-coded, and this color code is consistent across other panels. (B) Top: Microscope rotation angle over time corresponding to the vestibular sine stimulus (dashed line) and phase-shifted to compensate for the GCaMP6f sensor delay (black solid line). Bottom: Neuron-averaged traces for the four phase windows, color-coded according to their respective average phase shifts. (C) Maximum projection views of a representative example fish's phase map, registered to the Z-Brain reference brain (as depicted in E), divided into four phase intervals (i, ii, iii, and iv) as shown in (A). Each phase interval is displayed as maximum projection from left to midline and from dorsal to ventral. (D) Close-up view of the oculomotor (nIII) and trochlear (nIV) nuclei, revealing the spatial organization of their functional responses consistent with the anatomical projection patterns of these motoneurons to extraocular muscles (superior oblique (SO), inferior rectus (IR), superior rectus (SR), inferior oblique (IO)). The top and bottom panels correspond to the nose-up and nose-down positions, respectively, with schematics indicating the direction of stimulation (black arrow) and the direction of force exerted by the extraocular muscles (orange arrows) associated with pitch stimulation. (E & G) Four selected layers of the example fish's phase map were calculated from induced neuronal activity in response to pitch-tilts and roll-tilts, respectively. White arrowheads indicate vestibular spinal neurons. The dashed oval highlights roll-tilt responses in cerebellum, which are not present in the pitch-tilt maps. (F & H) Average phase maps of the pitch-tilt response (N = 8) and roll-tilt response (N = 8), respectively. Arrowheads indicate phasic neuronal populations. The dashed oval highlights roll-tilt responses in the rhombomere 1-3, which are absent in the pitch-tilt maps. Brain region contours extracted from the ZBrain atlas (13) depict the optic tectum (OT), torus longitudinalis (TL), habenula (Hab), cerebellum (Cer), tegmentum (Teg), oculomotor nucleus III (nIII) and IV (nIV), nucleus of the medial longitudinal fasciculus (nMLF), tangential nucleus (tVN), medial nucleus (mVN), vestibulospinal backfill (VS), and inferior olive (IO).
C: caudal; D: dorsal; L: left; R: right; Ro: rostral Refer also Video S1, S2 and S3 and Figure S3 and S2.

tral to the nMLF that could be neurons of the interstitial nucleus of Cajal.

Neural Responses to Stepwise Pitch-Tilt Stimuli. Alongside sinusoidal stimulation, we also analyzed the brain-wide response to step stimuli along the pitch-tilt axis in the same fish. The fish were moved in both nose-up and nose-down directions from their horizontal position at varying amplitudes (10°, 15°, 20°, illustrated in Figure 3). Each angular change had a 20-second dwell time, with motor operation at a peak angular velocity of 30°/s during step transitions.

Multilinear regression analysis identified three distinct neural response groups (Figure 3). The first group (blue) showed a mixed tonic-phasic response to nose-down pitch-tilts and a slight firing rate reduction for nose-up pitch-tilts. The second group (red) exhibited the opposite response, sensitive to nose-up tonic and phasic angular changes. The third group (yellow) displayed phasic responses to movements in both directions.

Figure 3 presents these neuron's locations in the representative example fish together with a density plot summarizing the results obtained from N = 10 fish. The nose-up responding neurons (orange) were mirror-symmetrically organized around the brain midline, predominantly in the tegmentum, with strong coverage of neurons of the nucleus of the medial longitudinal fascicle (nMLF) and the oculomotor nuclei (nIII and nIV). They were also found in the pretectum, ventral and dorsal thalamus, lateral cerebellum, and rhombencephalon, including the inferior olive, tangential vestibular nucleus, and all rhombomeres. In contrast, the nose-down responsive neurons (blue) showed a similar mirror symmetric organization but with fewer neurons in the oculomotor nucleus nIV and in

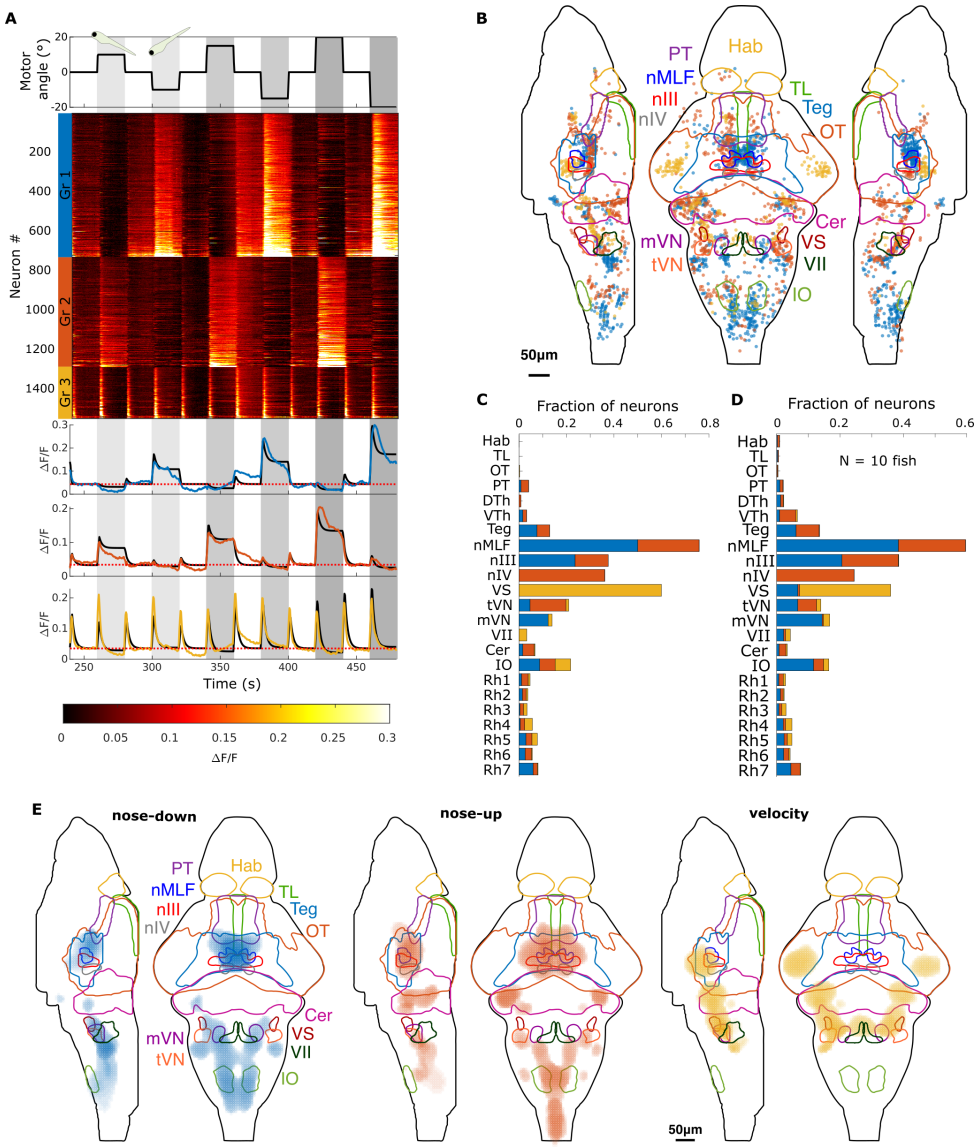

Fig. 3. Brain-wide Response to Step-wise Vestibular Stimuli along the Pitch-Tilt Axis. (A) Trial-averaged neuronal responses ordered by group affiliation determined through multilinear regression analysis against tonic and phasic components of the step stimulus. Neurons with strong responses to both tonic and phasic nose-up (nose-down) tilts are depicted in orange (blue). Top: Trace of the rotation angle α of the stimulus (in black). Positive angles correspond to nose-up, and negative angles correspond to nose-down. Middle: Rasterplot of trial-averaged responses of all identified neurons. Neuron indices are shown on the left, and their group membership is indicated by the color bar. Within each group, neurons are ranked based on the value of the group coefficient. Bottom: Mean trial-averaged response across all neurons of their respective groups, shown in their respective colors. The black line represents the average regression fit. (B) Spatial organization in the brain of neurons belonging to the three response groups. (C) Histogram showing the percentage of neurons in selected brain regions that belong to the different response groups. (D) Similar analysis to (C), but displaying cross-animal results (N = 10). (E) Cross-animal averaged response maps for the three response type groups (N = 10). Brain region contour lines are based on the ZBrain atlas: optic tectum (OT), torus longitudinalis (TL), habenula (Hab), cerebellum (Cer), tegmentum (Teg), oculomotor nucleus III (nIII), trochlear nucleus IV (nIV), medial longitudinal fasciculus nucleus (nMLF), tangential nucleus (tVN), medial nucleus (mVN), inferior olive (IO), pretectum (PT), dorsal thalamus (DTh), ventral thalamus (VTh), and rhombomeres 1-7 (Rh 1-7). See also Figure S4, S5, S6 and S7.

the cerebellum and with a more lateral distribution in rhombomere 4-5.

Neurons with purely phasic responses (yellow) were located in areas like the torus semicircularis, vestibulo-spinal neurons (VS), tangential vestibular nucleus (tVN), medial vestibular nucleus (mVN), inferior olive, and rhombomeres 1-5.

The cross-animal averaged response maps exhibit a consistent spatial organization, indicating a highly stereotypic neuronal arrangement (see Figure 3F).

Correlation Between Transgenic Line Expression and Vestibular Response Maps. By comparing our functional response maps with the transgenic line expression patterns collected in the Zebrafish Brain Browser (15), we have identified a significant overlap with the yt249 line's expression profile. To delve further into this correspondence, we crossed this Gal4 line with a UAS line expressing the GCaMP7a sensor (16), revealing that a substantial number of the labeled neurons were responsive to vestibular stimulation (refer to Figure S2).

The yt249 line effectively labels neurons spanning a broad spectrum of brain regions characterized, where a substantial part of labeled neurons are responding to vestibular stimuli. Particularly noteworthy, marked and responsive neurons are distributed across the corpus cerebelli, eminentia granularis, nuclear medial longitudinal fascicle (nMLF), the oculomotor nuclei (nIII and nIV), the torus semicircularis, statoacoustic ganglion, vestibulospinal neurons, lateral reticular nucleus, inferior olive, and the interstitial nucleus of Cajal (a neuronal population rostral to the nMLF and not labeled in the zBrain atlas).

Discussion

In this study, we conducted the first exhaustive brain-wide analysis of vestibular pitch-tilt response in larval zebrafish, leveraging an advanced rotating light-sheet microscope for precise rotations along both the pitch-tilt and the roll-tilt axis. This approach enabled a detailed examination of the brain's response to pitch-tilt stimulation, along with a comparative

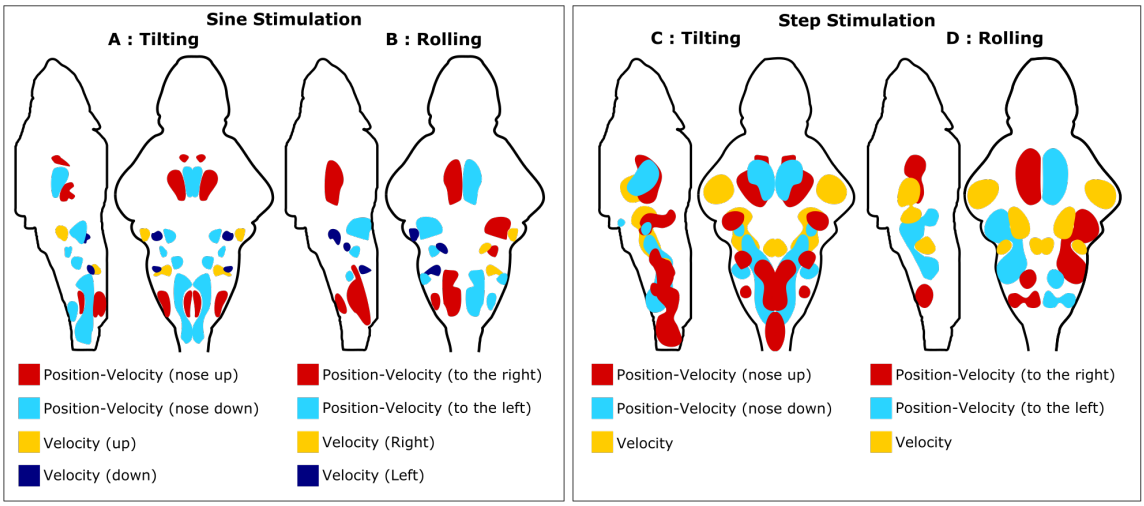

Fig. 4. Summary of Brain Regions Responsive to Sinusoidal and Stepwise Stimulation along Pitch and Roll Axes. This graphical representation was established based on the following data: (A) Figure 2F (B) Figure 2H (C) Figure 3E (D) Figure 5 from Migault et al. 2018 (5).

analysis of the roll-tilt response.

Our results reveal a widespread neuronal engagement throughout the brain during pitch-tilt stimulation, with neurons displaying a spatial arrangement that correlates with their sensitivity to specific tilt directions. This arrangement, mirrorsymmetric across both brain hemispheres, suggests the presence of finely tuned neural circuits for distinct movement responses to pitch-tilt stimuli, offering insights into the sensorymotor processing involved. These findings, including a side-by-side comparison with roll-stimuli responses, are comprehensively illustrated in Figure 4.

Asymmetry in Neuronal Recruitment During Pitch-Tilt Stimulation:

Cerebellum: Our study highlights notable asymmetries in brain region recruitment during pitch-tilt stimulation, particularly within the cerebellum. There was a pronounced cerebellar response to nose-up step stimuli, as opposed to a minimal average response to nose-down movements (Figure 3 F), a finding that was recently also reported for the specific response of Purkinje cells (11). This asymmetry is apparent in both kernel density maps and neuron proportion histograms. Contrastingly, during the sinusoidal pitch-tilt stimulation, cerebellar neurons were only sparsely activated, indicating a response variance to the smoothness and acceleration of the stimulus.

The directional asymmetry we observed intriguingly mirrors findings in vertical visual pursuit in primates and humans, where cerebellar Purkinje cells mainly respond to downward visual motion (17–19). This is relevant because nose-up pitch movements typically result in a perceived downward visual motion, linking vestibular and visual responses. This parallel between vestibular and visual responses suggests a complex interaction between these sensory systems, relevant particularly in gaze stabilization activities like the vestibulo-ocular reflex.

The inhibitory nature of Purkinje cells further suggests their role in facilitating downward eye movements by inhibiting muscles responsible for eye upward motion. This aligns with upward eye drifts seen in cerebellar atrophy patients (17) or primates with cerebellar lesions (20).

Furthermore, the consistent asymmetry in cerebellar responses to both vestibular and visual stimuli points to multimodal convergence within the cerebellum. This is in line with the cerebellum's known multimodal nature, highlighting its complex role in coordinating diverse sensory inputs.

Oculomotor Neurons: Our study's findings on the asymmetrical activation of oculomotor neurons in nIII and nIV align with recent backtracing studies mapping these neurons to their specific muscle targets. (14). The spatial organization of their responses reflects their role in controlling eye movements during pitch-tilt rotations. Notably, during nose-up rotations, nIV (innervating the superior oblique muscles) and the lateral part of nIII (affecting the inferior rectus muscles) coordinate for upward eye movement. In contrast, nose-down rotations involve the medial part of nIII, linked to the superior rectus and inferior oblique muscles, facilitating downward eye movements. These findings, illustrated in Figures Figure 2D and Figure S3, highlight the intricate neuromuscular control involved in ocular motion.

Caudal Hindbrain: In the caudal hindbrain, we also observed asymmetric recruitment of neurons: a medial-dorsal cluster responding to nose-up movements and two lateral strips responsive to nose-down movements. This differential activation pattern suggests the engagement of distinct postural motor programs, which likely play a role in compensating for destabilization in each direction. These findings illustrate how the caudal hindbrain contributes to the biomechanical adjustments required for maintaining balance and posture along the pitch-tilt axis.

Vestibular Nucleus: Asymmetry in neural recruitment within the vestibular nucleus has also been reported. Electrophysiological studies in cats revealed that 84% of secondary vestibular neurons are involved in vertical upward eye movements, in stark contrast to only 16% for downward move-

ments (21). Schoppik et al. (22), corroborated recently this asymmetry in larval zebrafish, finding that 85% thus a major part of these neurons anatomically project to the oculomotor nucleus nIV, which exclusively drives downward eye movements. However, our functional maps don't show this asymmetry. Instead, we found differential activation of the medial and tangential vestibular nuclei in response to nose-down and nose-up step stimuli. This pattern is specific to step stimuli, as sinusoidal responses showed negligible activity in these nuclei. We cannot exclude that the elav3 line might predominantly label vestibular neurons with fast phasic responses, leading to their representation in step responses and potentially obscuring the projection asymmetry of secondary vestibular neurons in our functional maps. Future investigations employing transgenic lines that specifically label vestibular secondary neurons could provide deeper insights into this discrepancy.

Comparative Analysis of Pitch and Roll Tilt Responses: In our study, we conducted a comparative analysis of neuronal responses to pitch-tilt and roll-tilt stimuli, utilizing the same fish for both sets of stimuli. The results of this comparison are visually depicted in Figure 4.

This approach highlights the contrasting neuronal activation patterns in response to different types of vestibular stimulation, providing a unique perspective on how these stimuli are processed within the fish brain.

Hindbrain Oscillator: Our study revealed that neurons located medially in rhombomeres 1-3 are selectively activated by roll-tilt stimuli. Intriguingly, these neurons align with the hindbrain oscillator network (23–25) and evidence accumulation circuits (26, 27), previously attributed roles in integrating lateral visual flow for decision-making, especially in directional swimming during spontaneous exploration. This suggests that, alongside visual processing, these neurons also integrate vestibular information, indicating multimodal integration within these circuits. Such integration could have significant implications for precise postural control, involving lateral tail movements, as suggested by Bagnall et al. (28). Notably, this activation pattern was absent in response to pitch-tilt stimuli, highlighting the response's specificity.

Vestibulospinal Neurons: Our study found vestibulospinal neurons on each side of the brain that are responsive to both pitch and roll stimuli, predominantly during nose-down tilts and ipsilateral ear-down rotations. However, it should be noted that these neurons might represent only a subset of all vestibulospinal neurons, due to the specificity of the elav3 labeling. This asymmetric response aligns with anatomical studies demonstrating that these neurons predominantly receive input from hair cells in the macula, tuned to rostral-lateral otolith displacements (29). Such responsiveness indicates their role in counteracting the postural challenges zebrafish typically encounter, particularly in situations of nose-down destabilization (12).

Cerebellum: The cerebellum's significant involvement during roll stimulation in fish underscores its essential role in maintaining a stable dorsal-up posture against destabilizing forces along the roll axis, particularly during swim bouts and turns. Unlike other movements, fish do not intentionally alter their body inclination along the roll axis for exploratory behavior. The cerebellum is likely continuously engaged in ensuring this constant dorsal-up orientation by modulating and refining motor actions. In contrast, body pitch angle control is less strict, often resulting in passive nose-down rotations of several degrees in pitch angle between consecutive bouts (12). This might be reflected in the cerebellum's relatively weaker recruitment during pitch-tilt vestibular stimulation and the low overlap between the two responses.

Overlap of Transgenic Line Expression Profiles with Vestibular Functional Maps: In our study, we also explored the correlation between our vestibular functional response maps and the expression patterns of various transgenic fish lines collected in the Zebrafish Brain Browser ((15)). This led to the identification of the yt249 transgenic line showing significant overlap with our functional maps. This line holds potential for future studies in tracing, optogenetics, or targeted ablations, which are crucial for a deeper understanding of the neural circuits involved in vestibular processing.

Limitations and future directions: Our study characterized brain-wide vestibular responses within a ±20-degree pitch-tilt range, reflecting common orientations during 3D exploration (12). Future work could expand to whole-orbit receptive fields using ratiometric imaging (7) to address movement artifacts in recordings over larger angular ranges. While our findings shed light on pitch-axis vestibular processing, further exploration is needed. Future research directions include exploring the brain centers initiating vestibular movements, identifying genetic cell types involved in vestibular processing, and understanding the functional significance of asymmetric responses during different tilts.

Our study advances the understanding of differential neuronal responses and asymmetries in pitch and roll-axis vestibular stimulation. Through extensive brain-wide assessments in larval zebrafish and analysis of transgenic fish line overlaps, we contribute to the growing knowledge of the vestibular system. The insights from this research are significant for comprehending postural control, spatial orientation, and the broader implications for neurological disorders associated with vestibular dysfunction (30).

ACKNOWLEDGEMENTS

We would like to thank the IBPS fish facility staff for their invaluable help.

We are also grateful to Carounagarane Dore for his important contribution to the realization of the mechanical parts of the light-sheet microscope.

We thank Misha Ahrens for providing the GCaMP6f line, Koichi Kawakami for the UAS:GCaMP7a line, and Harold Burgess for the yt249 line.

This project has received funding from the European Research Council (ERC) under the European Union's Horizon 2020 research and innovation program grant agreement number 715980 and by the ATIP-Avenir program from CNRS and INSERM.

S.C. received funding from the European Union's Horizon 2020 research and innovation program under the Marie Skłodowska-Curie grant agreement number 813457 ZEbrafish Neuroscience International Training Hub (ZENITH) as well as the Fin de thèse grant from the Fondation pour la Récherche Medicale (FRM).

G.M. was funded by a PhD fellowship from the Doctoral School in Physics, Ile de France (EDPIF).

Bibliography

1. Marian L. Dale, Fay B. Horak, W. Geoffrey Wright, Bernadette M. Schoneburg, John G. Nutt, and Martina Mancini. Impaired perception of surface tilt in progressive supranuclear palsy. *PLoS ONE*, 12(3):e0173351, 2017. doi: 10.1371/journal.pone.0173351.
2. Thomas Cronin, Qadeer Arshad, and Barry M. Seemungal. Vestibular Deficits in Neurodegenerative Disorders: Balance, Dizziness, and Spatial Disorientation. *Frontiers in Neurology*, 8:538, 2017. ISSN 1664-2295. doi: 10.3389/fneur.2017.00538.
3. Thomas Brandt, Michael Strupp, and Marianne Dieterich. Towards a concept of disorders of "higher vestibular function". *Frontiers in Integrative Neuroscience*, 8:47, 2014. ISSN 1662-5145. doi: 10.3389/fnint.2014.00047.
4. Yusra Mansour, Alyson Burchell, and Randy J. Kulesza. Central Auditory and Vestibular Dysfunction Are Key Features of Autism Spectrum Disorder. *Frontiers in Integrative Neuroscience*, 15:743561, 2021. ISSN 1662-5145. doi: 10.3389/fnint.2021.743561.
5. Geoffrey Migault, Thijs L. van der Plas, Hugo Trentesaux, Thomas Panier, Raphaël Candelier, Rémi Proville, Bernhard Englitz, Georges Debrégeas, and Volker Bormuth. Whole-Brain Calcium Imaging during Physiological Vestibular Stimulation in Larval Zebrafish. *Current Biology*, 28(23):3723 – 3735.e6, 12 2018. ISSN 0960-9822. doi: 10.1016/j.cub.2018.10.017.
6. Kyla R. Hamling, Yunlu Zhu, Franziska Auer, and David Schoppik. Tilt in Place Microscopy: a Simple, Low-Cost Solution to Image Neural Responses to Body Rotations. *The Journal of Neuroscience*, 43(6):936–948, 2023. ISSN 0270-6474. doi: 10.1523/jneurosci.1736-22.2022.
7. Masashi Tanimoto, Ikuko Watakabe, and Shin-Ichi Higashijima. Tiltable objective microscope visualizes selectivity for head motion direction and dynamics in zebrafish vestibular system. *Nature communications*, 13(1):7622, 2022. doi: 10.1038/s41467-022-35190-9.
8. Takumi Sugioka, Masashi Tanimoto, and Shin-Ichi Higashijima. Biomechanics and neural circuits for vestibular-induced fine postural control in larval zebrafish. *Nature communications*, 14(1):1217, 2022. doi: 10.1038/s41467-023-36682-y.
9. Itia A Favre-Bulle, Gilles Vanwalleghem, Michael A Taylor, Halina Rubinsztein-Dunlop, and Ethan K Scott. Cellular-Resolution Imaging of Vestibular Processing across the Larval Zebrafish Brain. *Current Biology*, 28(23):3711 – 3722.e3, 12 2018. doi: 10.1016/j.cub.2018.09.060.
10. Natalia Beiza-Canelo, Hippolyte Moulle, Thomas Pujol, Thomas Panier, Geoffrey Migault, Guillaume Le Goc, Pierre Tapie, Nicolas Desprat, Hans Straka, Georges Debrégeas, and Volker Bormuth. Magnetic actuation of otoliths allows behavioral and brain-wide neuronal exploration of vestibulo-motor processing in larval zebrafish. *Current Biology*, 33(12):2438–2448.e6, 2023. ISSN 0960-9822. doi: 10.1016/j.cub.2023.05.026.
11. Franziska Auer, Katherine Nardone, Koji Matsuda, Masahiko Hibi, and David Schoppik. Purkinje cells control posture in larval zebrafish (danio rerio). *bioRxiv*, 2023. doi: 10.1101/2023.09.12.557469.
12. David E Ehrlich and David Schoppik. Control of Movement Initiation Underlies the Development of Balance. *Current biology : CB*, 27(3):334 – 344, 02 2017. doi: 10.1016/j.cub.2016.12.003. du.
13. Owen Randlett, Caroline L Wee, Eva A Naumann, Onyeka Nnaemeka, David Schoppik, James E Fitzgerald, Ruben Portugues, Alix M B Lacoste, Clemens Riegler, Florian Engert, and Alexander F Schier. Whole-brain activity mapping onto a zebrafish brain atlas. *Nature methods*, 12(11):1039 – 1046, 2015. doi: 10.1038/nmeth.3581.
14. Marie R. Greaney, Ann E. Privorotskiy, Kristen P. D'Elia, and David Schoppik. Extraocular motoneuron pools develop along a dorsoventral axis in zebrafish, Danio rerio. *Journal of Comparative Neurology*, 525(1):65–78, 2017. ISSN 0021-9967. doi: 10.1002/cne.24042.
15. Gregory D Marquart, Kathryn M Tabor, Mary Brown, Jennifer L Strykowski, Gaurav K Varshney, Matthew C LaFave, Thomas Mueller, Shawn M Burgess, Shin-ichi Higashijima, and Harold A Burgess. A 3D Searchable Database of Transgenic Zebrafish Gal4 and Cre Lines for Functional Neuroanatomy Studies. *Frontiers in neural circuits*, 9(110):1566, 11 2015. doi: 10.1093/nar/gkr1288.
16. Akira Muto, Masamichi Ohkura, Gembu Abe, Junichi Nakai, and Koichi Kawakami. Real-Time Visualization of Neuronal Activity during Perception. *Current Biology*, 23(4):307–311, 2013. ISSN 0960-9822. doi: 10.1016/j.cub.2012.12.040.
17. Stefan Glasauer, Thomas Stephan, Roger Kalla, Sarah Marti, and Dominik Straumann. Up–Down Asymmetry of Cerebellar Activation During Vertical Pursuit Eye Movements. *The Cerebellum*, 8(3):385–388, 2009. ISSN 1473-4222. doi: 10.1007/s12311-009-0109-5.
18. L. S. Stone and S. G. Lisberger. Visual responses of Purkinje cells in the cerebellar flocculus during smooth-pursuit eye movements in monkeys. I. Simple spikes. *Journal of Neurophysiology*, 63(5):1241–1261, 1990. ISSN 0022-3077. doi: 10.1152/jn.1990.63.5.1241.
19. R. J. Krauzlis and S. G. Lisberger. Directional organization of eye movement and visual signals in the floccular lobe of the monkey cerebellum. *Experimental Brain Research*, 109 (2):289–302, 1996. ISSN 0014-4819. doi: 10.1007/bf00231788.
20. Amir Kheradmand and David S. Zee. Cerebellum and Ocular Motor Control. *Frontiers in Neurology*, 2:53, 2011. doi: 10.3389/fneur.2011.00053.
21. Y. Iwamoto, T. Kitama, and K. Yoshida. Vertical eye movement-related secondary vestibular neurons ascending in medial longitudinal fasciculus in cat I. Firing properties and projection pathways. *Journal of Neurophysiology*, 63(4):902–917, 1990. ISSN 0022-3077. doi: 10.1152/jn.1990.63.4.902.
22. David Schoppik, Isaac H Bianco, David A Prober, Adam D Douglass, Drew N Robson, Jennifer M B Li, Joel S F Greenwood, Edward Soucy, Florian Engert, and Alexander F Schier. Gaze-Stabilizing Central Vestibular Neurons Project Asymmetrically to Extraocular Motoneuron Pools. *The Journal of neuroscience : the official journal of the Society for Neuroscience*, 37(47):11353 – 11365, 11 2017. doi: 10.1523/jneurosci.1711-17.2017.
23. Misha B Ahrens, Michael B Orger, Drew N Robson, Jennifer M Li, and Philipp J Keller. Whole-brain functional imaging at cellular resolution using light-sheet microscopy. *Nature methods*, 10(5):413–420, May 2013. doi: 10.1038/nmeth.2434.
24. Sébastien Wolf, Alexis M Dubreuil, Tommaso Bertoni, Urs Lucas Böhm, Volker Bormuth, Raphaël Candelier, Sophia Karpenko, David G C Hildebrand, Isaac H Bianco, Remi Monasson, and Georges Debrégeas. Sensorimotor computation underlying phototaxis in zebrafish. *Nature Communications*, 8(1):651, 09 2017. doi: 10.1038/s41467-017-00310-3.
25. Timothy W Dunn, Yu Mu, Sujatha Narayan, Owen Randlett, Eva A Naumann, Chao-Tsung Yang, Alexander F Schier, Jeremy Freeman, Florian Engert, and Misha B Ahrens. Brain-wide mapping of neural activity controlling zebrafish exploratory locomotion. *eLife*, 5: e12741, 03 2016. doi: 10.7554/elife.12741.
26. Armin Bahl and Florian Engert. Neural circuits for evidence accumulation and decision making in larval zebrafish. *Nature Neuroscience*, 23(1):94–102, 2020. ISSN 1097-6256. doi: 10.1038/s41593-019-0534-9.
27. Elena I Dragomir, Vilim Štih, and Ruben Portugues. Evidence accumulation during a sensorimotor decision task revealed by whole-brain imaging. *Nature neuroscience*, 23(1):85 – 93, 12 2019. doi: 10.1038/s41593-019-0535-8.
28. Martha W Bagnall and David L McLean. Modular organization of axial microcircuits in zebrafish. *Science (New York, NY)*, 343(6167):197 – 200, 01 2014. doi: 10.1126/science.1245629.
29. Zhikai Liu, David G. C. Hildebrand, Joshua L. Morgan, Yizhen Jia, Nicholas Slimmon, and Martha W. Bagnall. Organization of the gravity-sensing system in zebrafish. *Nature Communications*, 13(1):5060, 2022. doi: 10.1038/s41467-022-32824-w.
30. C.D. Balaban. Chapter 3 Neurotransmitters in the vestibular system. *Handbook of Clinical Neurology*, 137:41–55, 2016. ISSN 0072-9752. doi: 10.1016/b978-0-444-63437-5.00003-0.
31. Nikita Vladimirov, Yu Mu, Takashi Kawashima, Davis V Bennett, Chao-Tsung Yang, Loren L Looger, Philipp J Keller, Jeremy Freeman, and Misha B Ahrens. Light-sheet functional imaging in fictively behaving zebrafish. *Nature methods*, 11(9):883 – 884, 2014. doi: 10.1038/nmeth.3040.
32. Torsten Rohlfing and Calvin R Maurer. Nonrigid image registration in shared-memory multiprocessor environments with application to brains, breasts, and bees. *IEEE trans. inf. technol. biomed.*, 7:16 – 25, 2003. doi: 10.1109/TITB.2003.808506.
33. Owen Randlett, Caroline L Wee, Eva A Naumann, Onyeka Nnaemeka, David Schoppik, James E Fitzgerald, Ruben Portugues, Alix M B Lacoste, Clemens Riegler, Florian Engert, and Alexander F Schier. Whole-brain activity mapping onto a zebrafish brain atlas. *Nat. Methods*, 12(11):1039 – 1046, 2015. doi: 10.1038/nmeth.3581.

Videos legends

Video S1 **Trial averaged response to sinusoidal pitch-tilt stimulation**

Video S2 **3D animated phase map to pith-tilt stimulus.**

Video S3 **3D animated phase map to roll-tilt stimulus.**

Method Details

Animal husbandry. All experiments were performed on 5-7 dpf larvae. The sex of the animals was not yet determined at this age, and was therefore not reported. Adult fish were maintained at 28°C in system water (pH 7-7.5 and conductivity between 300 and 350 μS) in the fish facility of the Institut de Biologie Paris-Seine. Eggs were collected in the morning and then kept in a Petri dish with E3 at 28°C under a 14h/10h light/dark cycle. Larvae were fed with rotifers from 5 dpf on. Calcium imaging experiments were carried out in two different transgenic lines: *elavl3:H2B-GCaMP6f* (31) and *y249:Gal4 ;UAS:GCaMP7a* (15, 16), both in nacre background. Experiments were approved by Le Comité d'Éthique pour l'Expérimentation Animale Charles Darwin C2EA-05 (02601.01 and #32423-202107121527185 v3).

3D Printing. The bracket and all other custom parts (1B, cyan elements) were printed using an Original Prusa MINI+ 3D printer, and we used Prusament PETG filament with a layer quality of 0.2mm and a density of 80%. The 3D design file is open source and can be accessed at `https://a360.co/2U1KBoH`.

Sample Preparation. First, the fish were paralyzed by immersing them for 75 seconds in 25 μL of a 1 mg/mL α-bungarotoxin solution (Thermo Fisher Scientific) in E3 medium. They were then transferred to pure E3 medium and left for 30 minutes to ensure the absence of motor activity while maintaining a normal heartbeat. Subsequently, the larvae were carefully placed in a 2% low-melting agarose solution (Sigma-Aldrich) and tail-first drawn into a 1 mm inner diameter glass capillary tube using a plunger. After this step, the agarose was cut directly rostral to the fish.

Acquisition Protocol. We conducted volumetric imaging at a rate of 2.5 stacks per second, covering 25 brain sections. Each section had an inter-slice distance of 10 μm and a pixel size of 1.2x1.2 μm^2.

Quantification and Statistical Analysis. For the characterization of the setup mechanical stability during microscope rotation, the processing of functional light-sheet data, the registration onto the z-Brain atlas, the generation of the phase maps, and the generation of the average cluster density maps we followed the protocols described in Migault et al. (5).

Estimation of Decay Time Constant for the Nuclear H2B-GCaMP6f Calcium Sensor. In our previous work, we estimated the phase shift induced by the GCaMP6s reporter to be -1.35 ± 0.05 rad (5). In this study, we estimated the phase shift for the GCaMP6f reporter by comparing neural response phases in the trochlear nucleus during rolling stimulation with those from larvae expressing GCaMP6s. Due to its consistent and large neuronal responses, the trochlear nucleus was chosen for this comparison. The observed phase shift difference between GCaMP6s and GCaMP6f was 0.20 ± 0.05 radians. Consequently, we deduced the phase shift introduced by GCaMP6f to be -1.15 ± 0.10 radians. This translates to a decay time of $\tau = -\omega^{-1} \tan\phi = 1.78 \pm 0.80$ seconds, significantly smaller than the decay time of 3.5 ± 0.7 seconds for GCaMP6s, as we previously estimated.

Regression analysis of neural response properties. We conducted the multilinear regression analysis using a modified version of the protocol from Migault et al. (2018). In addition to two angular position regressors, we introduced four new regressors based on the microscope's velocity signal. These regressors, defined by the angular velocity's direction, differentiate between movements away from or towards the preferred dorsal-up orientation (see Figure S4). This enhanced the analysis's precision. Neurons were classified as responsive if their regression coefficients and T-scores were above the 94th percentile for at least one of the six regressors. The analysis involved convolving all six regressors with the H2B-GCaMP6f response kernel, estimated as a single exponential decay with a τ = 1.78 s decay time (see Figure). To identify highly responsive neurons, we set a threshold at the 94th percentile for both the regression coefficient and T-score distributions. Neurons that fell within the intersection of both 94th percentiles were clustered, indicating a robust response to the regressor (manifested as a high coefficient) and a significant explanation of neuron variance (reflected in high T-scores). Supplementary Figures S5 and S6 offer an illustration of this selection procedure.

Rescource Table

REAGENT OR RESOURCES	SOURCE	IDENTIFIER
Chemicals		
2D Galvo Mirror Systems	Thorlabs	GVS01@
Low melting point agarose	Sigma-Aldrich	A9414-50G
α-bungarotoxin	Thermofisher Scientific	B-1601
Experimental Models: Organisms/Strains		
Tg(elav3-H2B:GCaMP6f)		Vladimirov et al., 2014(**?**)
y249:Gal4 ;UAS:GCaMP7a		Marquart et al., 2015 and Muto et al., 2013 (15, 16)
Software and Algorithms		
Matlab	The MathWorks	https://www.mathworks.com/products.html
Labview	National Instruments	https://www.ni.com
CMTK	Rohlfing and Maurer, 2003 (32)	https://www.nitrc.org/projects/cmtk/
FIJI	(ImageJ) NIH	https://fiji.sc/
Z-Brain atlas	Randlett et al., 2015 (33)	https://zebrafishexplorer.zib.de/home/

Table 1. Key resource table

Supplementary Figures

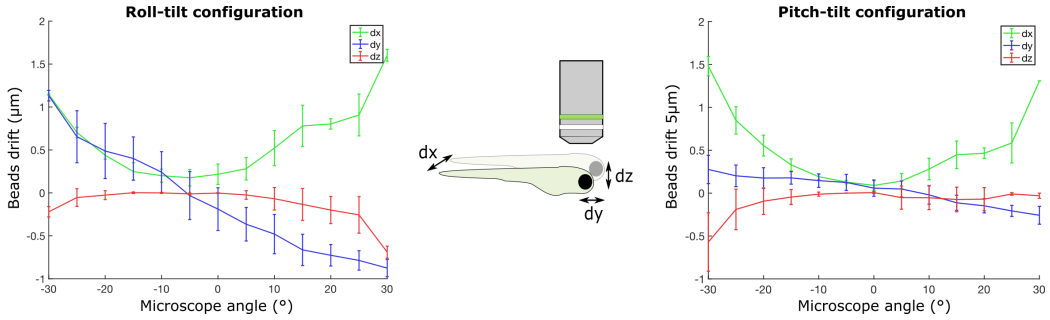

Fig. S1. Characterization of the Mechanical Stability of the Imaging System in Roll- and Pitch-Tilt Configuration. Related to Figure 1. Mechanical stability assessment along the three directions (dx, dy, and dz) as a function of the microscope rotation angle. Error bars represent the standard deviation (SD) of measurements, with N = 5. The microscope rotation spans from -30° to +30° for the characterization along the roll- and pitch-tilt axes.

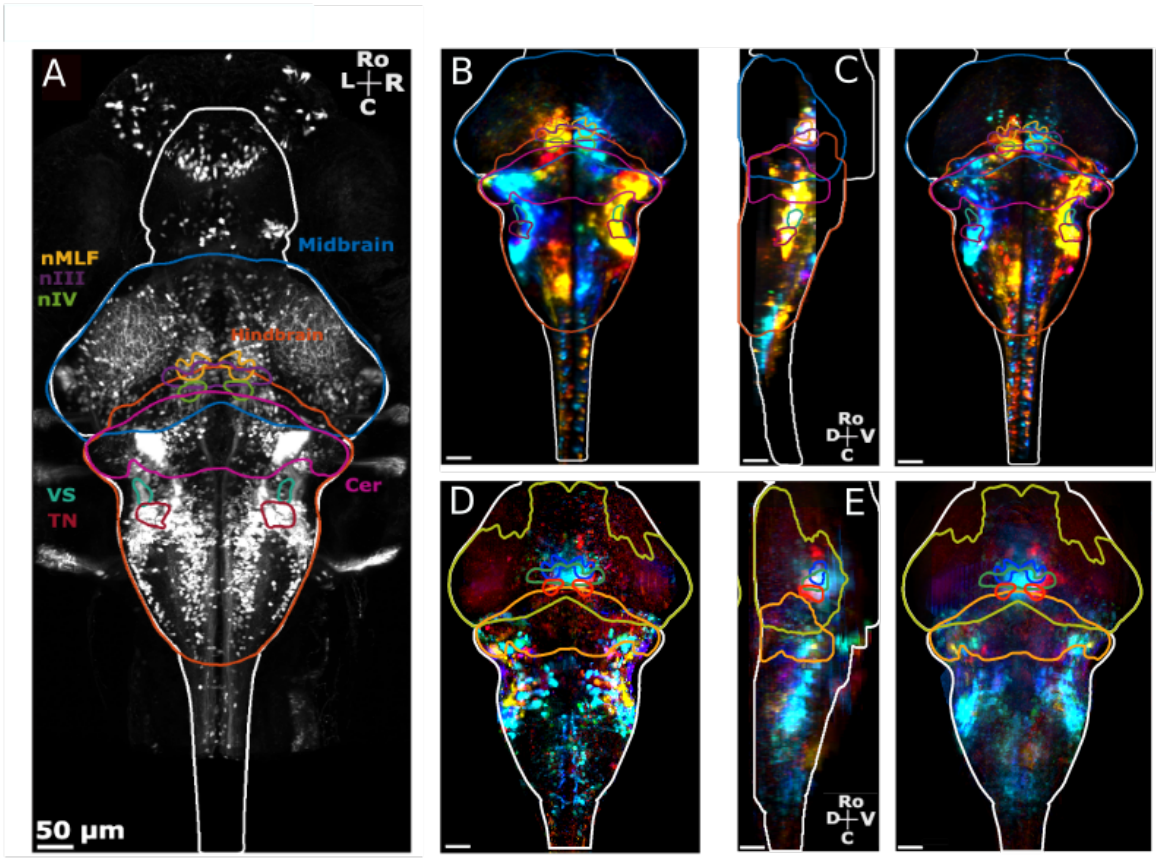

Fig. S2. Functional Brain-wide Response to Sinusoidal Roll in the y249Et Line. Related to Figure 2. (A) Z-projection of the anatomical stack of the Y249Et transgenic line downloaded from the ZebraBrainBrowser library and mapped onto the zBrain atlas. (B) Z-projection example-fish phase map displaying neurons active during sinusoidal roll. Yellow-orange regions indicate activity during right-ear-down roll, while blue and cyan indicate activity during left-ear-down roll. (C) Side and dorsal views of the average phase map (N = 6 fish). (D) Z-projection example-fish phase map displaying neurons active during sinusoidal tilt-axis stimulation. Red regions indicate activity during nose up pitch, while cyan indicates activity during nose down pitch. (E) Side and dorsal projections of the average phase map (N = 10 fish). Brain region contour lines are based on the ZBrain atlas: cerebellum (Cer), oculomotor nucleus III (nIII), trochlear nucleus IV (nIV), medial longitudinal fasciculus nucleus (nMLF), tangential nucleus (TN), and spinal backfill vestibular population (VS). Scale bar = 50 μm.

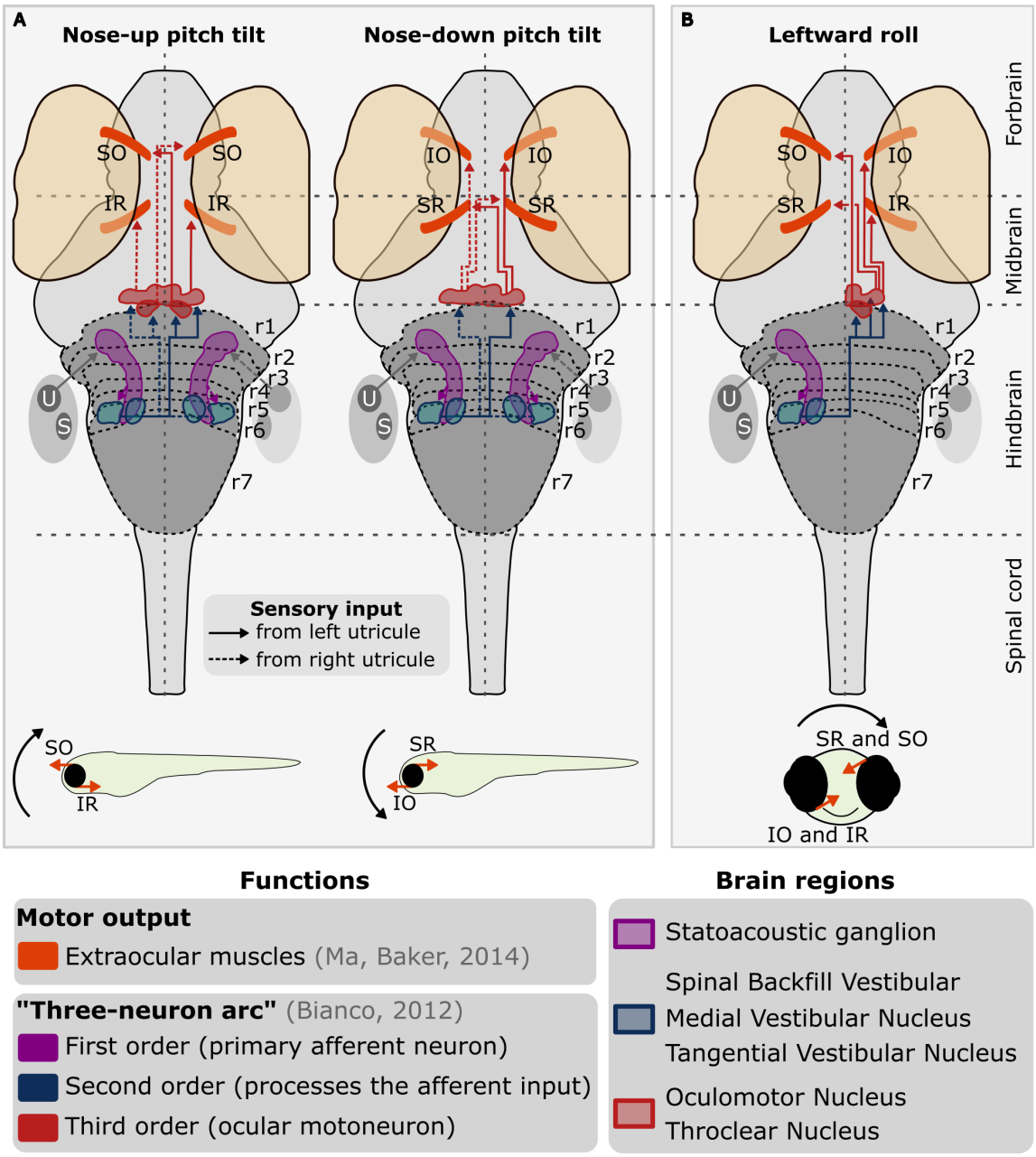

Fig. S3. Schematic of Neural Network and Behavioral Responses during Vestibulo-Ocular Reflex (VOR). Related to Figure 2. Schematic representation of the neural network involved in the angular vestibulo-ocular reflex (VOR) during pitch-tilt (A) and roll-tilt (B), accompanied by corresponding behavioral response patterns (black arrow indicates stimulation direction, while orange arrows depict the force direction exerted by the extraocular muscles). Key elements include the extraocular muscles (superior rectus, SR; inferior rectus, IR; inferior oblique, IO; and superior oblique, SO), utricle, U; saccule, S; and rhombomeres, r1 to r7.

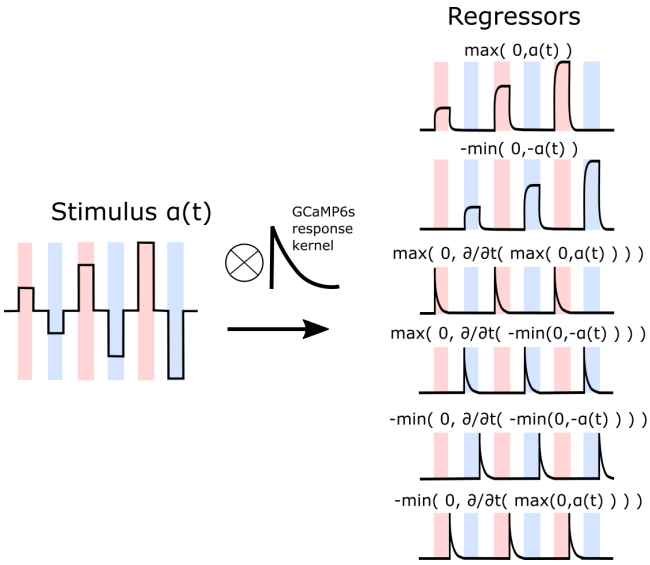

Fig. S4. Construction of Regressors from the Stimulus. Related to Figure 3. This graphical representation demonstrates the sequential process of convolving the stimulus signal, $\alpha(t)$ with the kernel representing the temporal dynamics of the GCaMP calcium sensor. The subsequent creation of positive tonic and phasic components is depicted, resulting in the formation of the six distinct regressors utilized in the multilinear regression analysis.

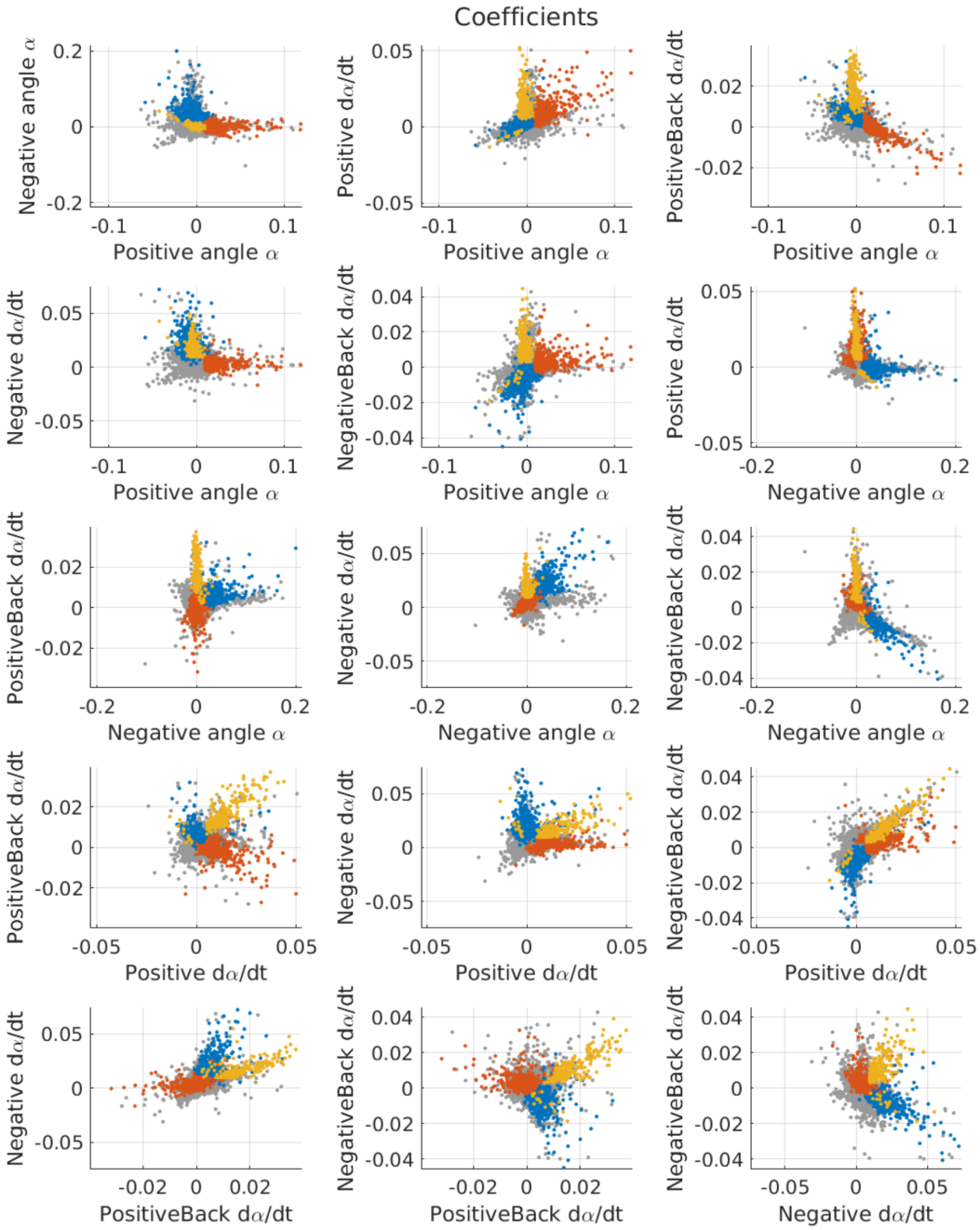

Fig. S5. Scatter Plots of Regression Coefficients for Identified Neuronal Response Groups. Related to Figure 3. Scatter plots representing the regression coefficients corresponding to the three identified groups of neuronal responses, as illustrated in Figure 3. Neurons not categorized within these three groups are denoted by gray dots.

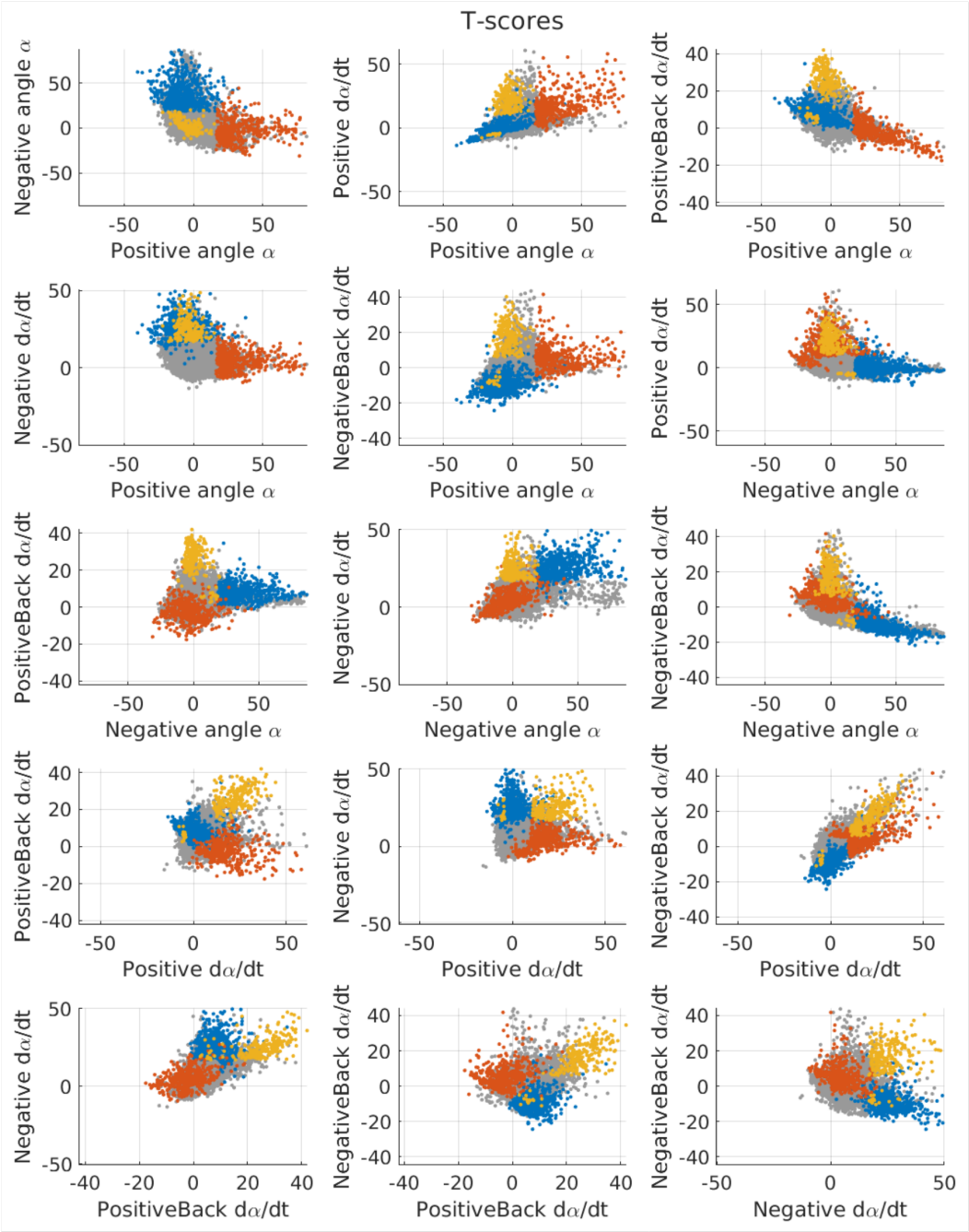

Fig. S6. Scatter Plots of Regression T-Scores for Identified Neuronal Response Groups. Related to Figure 3. Scatter plots depicting the regression T-scores associated with the three identified groups of neuronal responses, as depicted in Figure 3. Neurons falling outside of these three groups are represented as gray dots.

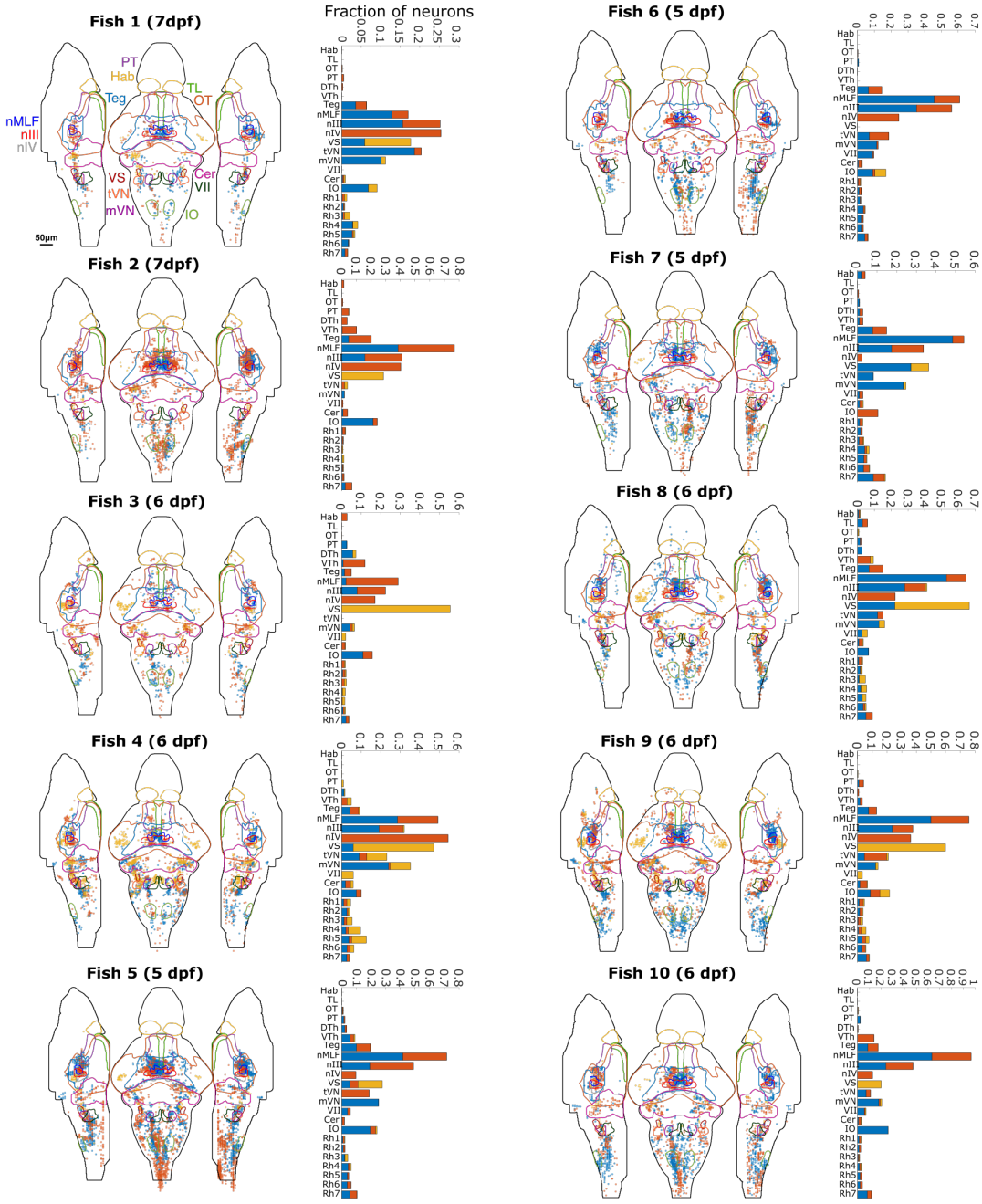

Fig. S7. Regression Results Visualization and Histograms of Neuronal Response Groups. Related to Figure 3. Visualizations of the regression results for the ten fish used in the average depicted in Figure 3. Accompanying histograms illustrate the fraction of neurons belonging to the three identified groups within specific brain regions.